Case Studies in Construction Materials 15 (2021) e00593

Contents lists available at ScienceDirect

Case Studies in Construction Materials

journal homepage: www.elsevier.com/locate/cscm

Experimental investigation of crack width variation along the concrete cover depth in reinforced concrete specimens with ribbed bars and smooth bars

Chavin N. Naotunna *, S.M. Samindi M.K. Samarakoon, Kjell T. Fosså

Department of Mechanical and Structural Engineering and Material Science, Faculty of Science and Technology, University of Stavanger, Stavanger, Norway

ARTICLE INFO

Keywords:
RC specimens
Crack width
Crack pattern
Concrete cover depth
Ribbed reinforcement
Smooth bars
Experiments
Epoxy injection

ABSTRACT

Crack width variation along the concrete cover depth has been studied from the past for better understanding of the cracking phenomenon in reinforced concrete (RC) structures. Previous studies have highlighted important cracking behaviors like internal cracks. The behavior of 'slip' between the reinforcement and concrete and the formation of a nonuniform crack face along the concrete cover depth are still not very clearly understood. An experimental program has been conducted to study the crack width variation along the cover depth in concrete prisms reinforced with a central ribbed bar and smooth bar, by varying the concrete cover depths. Both in specimens with smooth bars (SS) and specimens with ribbed bars (SR), crack width is larger on the concrete surface than at the steel bar surface. The crack width at the reinforcement is considerably larger in the SS than in the SR. In the SR, the crack width increases from the reinforcement along the cover depth bi-linearly, while, in the SS, it increases linearly. For the SR, the aforementioned behavior is due to the occurrence of internal cracks. In the SS, significant slip has been identified at the reinforcement and concrete interface, whereas negligible slip has been observed in the SR. A surface crack width calculation model has been developed, considering both the strain difference and the effect of the nonuniform crack face along the concrete cover depth. Its predictions showed good agreement with the experimental surface crack widths from the conducted study and with the results from the experiments in literature.

1. Introduction

To understand the cracking behavior of RC specimens, crack width variation along the concrete cover depth has been studied and documented since 1968 [1]. Previous studies on crack width variation along the concrete cover depth have mainly employed two different experimental methods. One method is to measure the relative displacement between reinforcement and concrete at the ends of the specimen, using linear variable differential transducer (LVDT) gauges. Such studies are reported in Tammo and Thelandersson [2,3] and in Yannopoulos [4]. However, several difficulties can be identified in this type of experiment. The 'cone failure' that can occur at the end of the specimen can cause readings which are taken at the vicinity of the reinforcement to be misguided. On the other hand, it is difficult to measure the deformation just above the reinforcement, since placing the LVDT gauges consumes several

* Corresponding author.
E-mail address: chavin.guruge@uis.no (C.N. Naotunna).

https://doi.org/10.1016/j.cscm.2021.e00593
Received 3 February 2021; Received in revised form 1 June 2021; Accepted 5 June 2021
Available online 8 June 2021

millimeters. For example, Tammo and Thelandersson [2,3] and Yannopoulos [4] obtained readings closest to the reinforcement at 4.5 mm and 2.2 mm away from the reinforcement, respectively. The other method is to seal the crack with a high strength (to avoid shrinking after load is released) and low viscosity (to penetrate through fine gaps) epoxy and observe the crack after cutting the RC specimen. Husain and Ferguson [1], Beeby [5] and Borosnyoi and Snobli [6] observed the crack width variation along the concrete cover depth by using this method, which involves several cost- and time-consuming activities, compared to the first method. It is necessary to keep the load in the cracked specimen until the injected epoxy is hardened (e.g., 20 h for the conducted test reported in this article). Other than that, it is necessary to cut the RC specimens to obtain the internal crack width measurements. However, the results from both these methods have concluded that, in RC specimens with ribbed bars, the crack width at the reinforcement is significantly smaller than the crack width at the concrete surface.

Analytical [7] or semi-analytical crack width calculation models, as in Eurocode 2 [8] or Model Code 2010 [9], predict the crack width as the extension occurring due to the strain difference between reinforcement and concrete between two cracks. Therefore, the crack width is obtained by multiplying the crack spacing with mean strain difference between reinforcement and concrete. Such models assume a constant crack opening through the cover depth [6,9]. However, according to the results of the aforementioned experiments, a contradictory observation is given that the crack width at the reinforcement is significantly smaller than the crack width at the concrete surface. Borosnyoi and Snobli [6] and Caldentey et al. [10] have explained that this small crack width at the reinforcement is due to the presence of Goto cracks (internal cracks/secondary cracks) [11]. These secondary cracks are mostly formed at the locations of ribs within the concrete, at the vicinity of primary cracks [11–13]. As the concrete strain is accumulated at these secondary cracks, it can be considered that the width of the primary cracks at the reinforcement is reduced. Due to the strong bond between the ribbed reinforcement and concrete, the strain incompatibility which occurs after cracking would accumulate in these internal cracks [14].

Crack spacing calculation models are mainly based on three theories: namely, bond-slip theory, no-slip theory and combined theory. The bond-slip theory assumes that a bond failure would occur at a crack, and therefore a slip would occur between reinforcement and concrete [15]. It is assumed that the slip is at its maximum at the crack and, after a certain distance from the crack, the slip would be zero. By considering the force equilibrium between a crack and a zero-slip location, a crack spacing model can be developed [16]. However, the no-slip theory assumes a perfect bond between reinforcement and concrete, with no possibility of a slip occurring between reinforcement and concrete at the crack [17]. The combined theory [18] considers the effect of slip, as well as the no-slip effect. A detailed study of these theories is mentioned in Naotunna et al. [19]. It is important to identify the crack theory (bond-slip theory or no-slip theory) which is more relevant to the actual cracking behavior of RC specimens, because the crack spacing governing parameters can be identified based on these theories.

Tammo and Thelandersson [3] mentioned that concrete cover depth has two main influences on the crack width. The first influence of concrete cover depth is the effect on the crack spacing. The second is the formation of a non-uniform crack face, which causes the surface crack width to increase. In other words, this effect is discussed as shear lag in several pieces of literature [6,20,21]. The shear-lag effect is not considered or mentioned in any of the widely used crack width calculation models. According to the literature, the effect of shear lag is dominant with the increase in concrete cover depth [6,20,21]. In the first complete draft of Model Code 2010, a formula was given which included the shear-lag effect. However, the effect of shear lag is not taken into account in the final draft, and the proposed crack width calculation model is valid up to a cover depth of 75 mm. It is vital to use large concrete cover depths when structures are located in an adverse environment and have a very long service life (200 or 300 years) [22,23]. According to the Norwegian Public Road Administration guidelines [24], the current requirement for concrete cover depth can be as large as 120 mm. Furthermore, the Hafrsfjord bridge in Norway has been constructed with a 90-mm cover depth [25]. Therefore, it is important to improve the existing crack width calculation models to be used in specimens with large concrete cover depths.

This study of crack width variation along the concrete cover depth has several objectives. One of the main ones is to study the behavior of slip, as the widely used crack spacing models have been developed based on theories considering slip. Another objective is to identify shear-lag effect, which can be more important in specimens with large concrete cover depths. Therefore, an experimental program has been conducted to observe the crack width variation along the concrete cover depth. Concrete prisms reinforced with a

Fig. 1. Reinforcement bars surfaces of 16 mm bars used for the SS and SR.

central bar were tested with different concrete cover depths, varying from 20 mm to 80 mm. For the better understanding and comparison of the cracking behaviors, specimens were cast with both ribbed bars and smooth bars. Then, in order to check whether the surface crack width has an additional effect, other than from the strain difference within the crack spacings, a crack width calculation model was developed by considering the effect of shear lag. A comparison has been made between the experimental surface crack widths and the predictions from the proposed crack widths.

2. Materials and methods

Concrete prisms, with a length of 650 mm and reinforced with a central reinforcing bar, were cast. The central reinforcing bars were 16 mm in diameter, and both ribbed and smooth surface bars were selected. The selected reinforcement bars are shown in Fig. 1. Table 1 gives the specimen sizes and concrete cover depths used in the experiment. For each case, two identical specimens were cast and tested. For the ribbed bar, the reinforcement grade was B500NC according to the NS 3576-3 standard [26], with a characteristic yield strength ($f_{yk,\ 0.05}$) of 500 MPa and Young's modulus of 200 GPa. For the SS, the smooth bar grade was S355J2 according to the NS 10219 standard [27], with a characteristic yield strength ($f_{yk,\ 0.05}$) of 355 MPa and Young's modulus of 210 GPa. The focus of the study is to observe the crack width variation along the concrete cover depth. When the crack widths are large, it would make the epoxy injection process to seal the crack easier. For the SS with a cover depth of 20 mm, the crack widths are relatively small due to the lower cover depth. Therefore, in order to ease the epoxy injection, the specimens were loaded up to 400 MPa, after confirming that the yield strength of smooth bars in three samples are above 400 MPa with an average of 425 MPa. The studies conducted by Cadoni et al. [28] and Duarte et al. [29] had obtained the same conclusion from their experiments, that the yield strength of S355J2 steel is above 400 MPa.

The mean $\phi 150 \times 300$ mm cylindrical compressive strength of concrete after 28 days of casting was 24.3 MPa, and the mean splitting tensile strength was 2.2 MPa. The top surface of the specimens (the surface which has not touched the formwork) was covered with polyethene on the first day, just after casting. The specimens were unmolded on the next day, and necessary measures were taken to cure the specimens, to control shrinkage. Next, the specimens were tested in axial tension with a monotonical loading rate of 0.5 mm/min, using the 'Instron 5985' machine. The specimens with ribbed reinforcement were loaded up to 100 kN, and the specimens with smooth bars were loaded up to 80 kN, to prevent yielding of the reinforcement. The specimens were loaded up to this value, since the crack sealing process would be easier with larger crack widths. This would make the crack sealant epoxy penetrate completely throughout the crack. The specimens were axially loaded with a 0.5-mm/min rate, after reaching the aforementioned maximum value, the load was kept constant for 24 h. This time lapse was required for the sealing of the crack, including the hardening of the crack sealant epoxy.

The loading procedure is allocated by the managing software of the loading machine, 'Instron Bluehill'. As mentioned, the specimens were loaded by means of the displacement control method. Then the displacement was kept constant for 24 h, until the applied load had reached the aforementioned threshold values (100 kN for specimens with ribbed bars and 80 kN for specimens with smooth bars). During this period, the cracks that appeared were sealed with a crack sealant epoxy. Sealing a crack was conducted in two main steps. In the first step, surface packers were pasted in the four faces, and the surfaces of the cracks on the four sides of the specimen were sealed with a rapidly hardening epoxy. Surface packers of the necessary size were produced by 3D printing in the University of Stavanger laboratory. Fig. 2 shows the surface packers used for the experimental program. By conducting a trial test, an epoxy named 'super lima' was selected as the surface sealant rapid hardening epoxy. After applying this surface sealant epoxy, nearly 45 minutes were required for hardening. Fig. 3 shows the loaded RC tie with the fixed surface packers. After hardening the surface sealant epoxy with the surface packers, the second step begins. The cracked concrete particles and the dust inside the crack were removed with a portable air pump. Then the cracks were sealed by injecting a crack sealant epoxy through the surface packers. For this purpose, an epoxy named 'Mapepoxy BI-IMP', which has been certified by the European concrete repair standard EN 1504-5 [30], was used. This epoxy consisted of two components, which had to be mixed in the prescribed ratio (component A: component B, mixing ratio 7:3). The mixture had a viscosity of nearly 110 mPa.s; after hardening, it had a compressive strength of 65 MPa. The next important property of this product is that it polymerizes without shrinkage. After mixing, the epoxy was injected into the cracks with a syringe through the previously fixed surface packers. Fig. 4 shows how the epoxy was inserted into the crack. From the trial test, it was identified that it takes around 20 h to harden the epoxy. After hardening the epoxy, the load in the testing apparatus was released and specimens were removed from the apparatus. No difference could be observed in the surface crack widths before and after releasing the applied load. Therefore, it can be assumed that, after the cracks had been sealed using this method, the crack widths did not change after the load was released. When cutting the sealed specimen, the epoxy could be confirmed to have penetrated throughout the whole crack.

Table 1
Sizes of the specimens and concrete cover depths.

Specimen	Concrete cover (mm)	Specimen width × height × length (mm × mm × mm)
Specimens with ribbed bars (SR)	40	96 × 96 × 650
	60	136 × 136 × 650
	80	176 × 176 × 650
Specimens with smooth bars (SS)	20	56 × 56 × 650
	40	96 × 96 × 650
	60	136 × 136 × 650

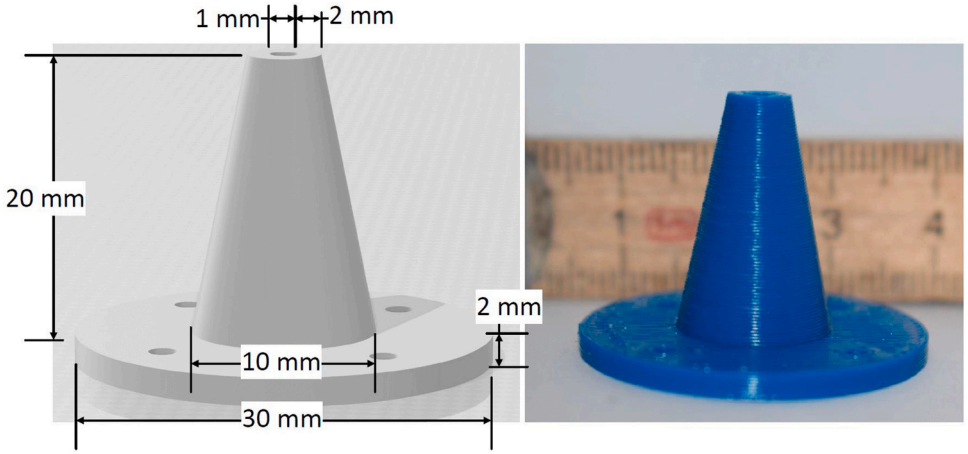

Fig. 2. Surface packers used to inject epoxy.

Fig. 3. Loaded RC tie after fixing the surface packers.

The next step was to cut the specimens, to observe how the crack width varied throughout the concrete cover depth. Specimens were cut, using a 'Diamant-Cedima' concrete cutter, with a cutting blade thickness of nearly 1 mm. Fig. 5 shows how the specimens were cut to observe the crack width propagation along the concrete cover. One sealed crack consists of eight cutting surfaces. Since there are several numbers of cutting surfaces, each cutting surface was coded. Fig. 6 shows the codes used to identify the cutting surface. In the specimens with ribbed bars (SR), two cracks per specimen from r.40.1 and r.40.2 and one crack per specimen from r.60.1, r.60.2 and r.80.2 were sealed and observed. In the specimens with smooth bars (SS), two cracks per specimen from r.20.1 and r.20.2 and one crack per specimen from s.40.1 and s.40.2 were sealed and observed. No cracks could be generated from s.60.1 and s.60.2, since the specimen lengths were not sufficient to generate cracks.

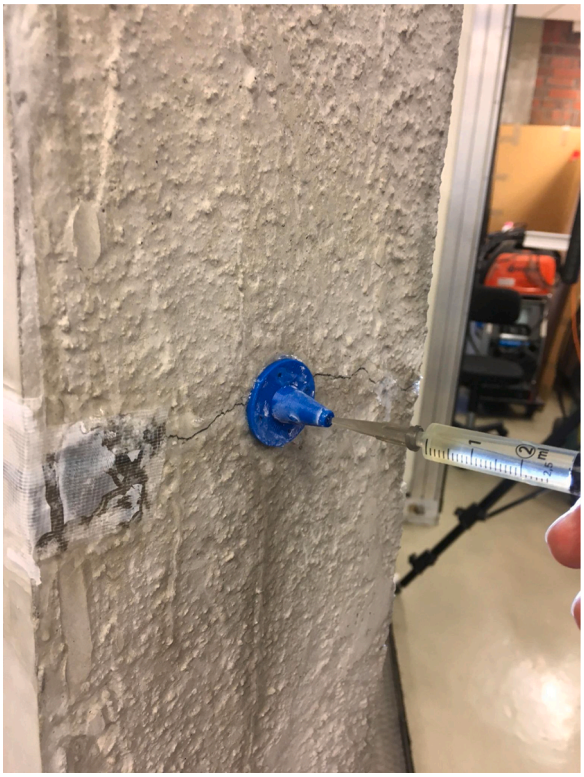

Fig. 4. Inserting the Mapepoxy BI-IMP to the crack through the surface packers.

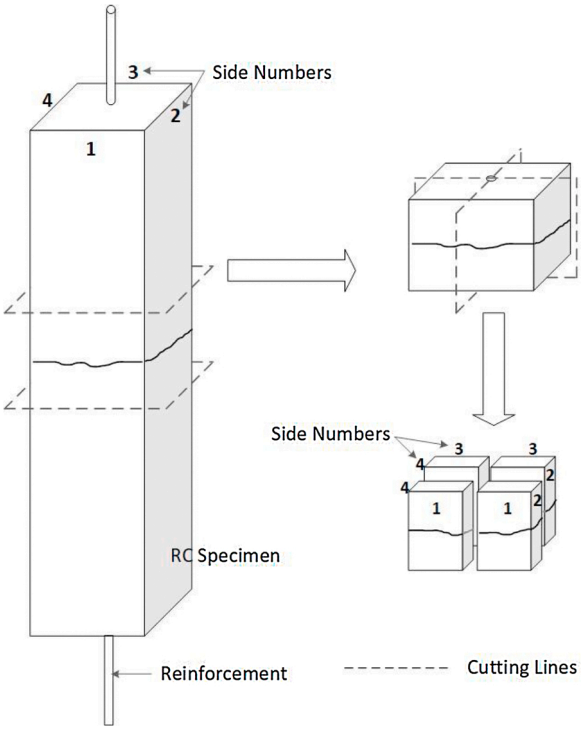

Fig. 5. Cutting of RC ties to observe the crack width propagation along the concrete cover.

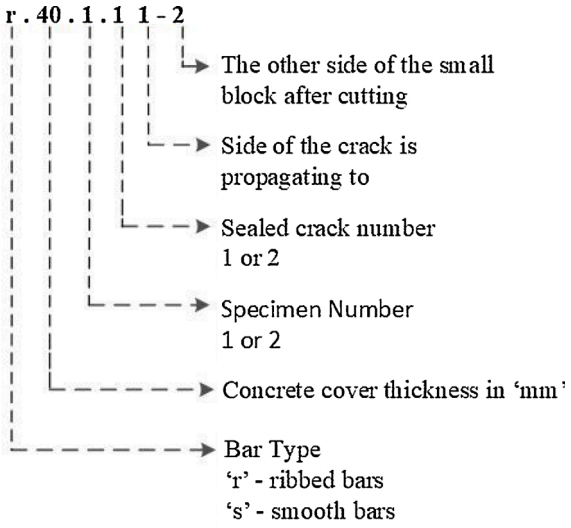

Fig. 6. Identification of the cutting surface.

3. Crack width measurements

In each cutting surface, crack widths were measured along the concrete cover depth at 2-mm intervals. The measurements were obtained using two methods. In the first method, initially photos of the cracks in the cutting surface were taken from a digital single-lens reflex camera (DSLR camera) with a 50-mm macro lens. Then the images were analyzed, using a computer program named 'Fiji ImageJ' [31]. The measurements taken from this method have an accuracy of 1 μm. From this program, the images can be calibrated and meshed with 2-mm grid sizes, to ease the measuring of crack widths. Fig. 7(a) shows an example of how the crack width measurements were taken with the Fiji ImageJ software. These obtained measurements were further confirmed by comparison with the measurements obtained with the 'Dino-Lite' digital microscope [32]. Fig. 7(b) shows the crack width measurements with the Dino-Lite digital microscope. As can be observed in Fig. 7(b), since the field of view of the Dino-Lite digital microscope is small, it is mainly used to confirm the measurements obtained from the first method. The measurements obtained from the Dino-Lite digital microscope have an accuracy of 1 μm.

As shown in Figs. 5 and 6, cutting surfaces 1-2 and 1-4 of a crack denote the same crack position, which is propagating to side 1. Similarly, cutting faces 2-1/2-3, 3-2/3-4 and 4-1/4-3 of a crack denote the same positions which are propagating to sides 2, 3 and 4, respectively. However, slight changes can be observed between the crack width measurements, even obtaining the readings of two cutting surfaces of the same crack, which are propagating to the same side (e.g., crack width measurements of cutting surfaces 1-2 and 1-4). One reason for this is that the position of the measurement point (2-mm steps) is not similar in both cutting faces. The other reason can be the 1-mm width of the cutting blade, which is wearing from the specimen while cutting. For example, there is a 1-mm gap between cutting faces 1-2 and 1-4 of a sealed crack. For this reason, the crack width measurements of two cutting faces which are propagating to the same side have been averaged (e.g., cutting phases 1-2 and 1-4 are averaged to represent the crack propagation to side 1). Therefore, as shown in Figs. 8 and 9, each sealed crack has four sets of readings, corresponding to each side of the face. In some

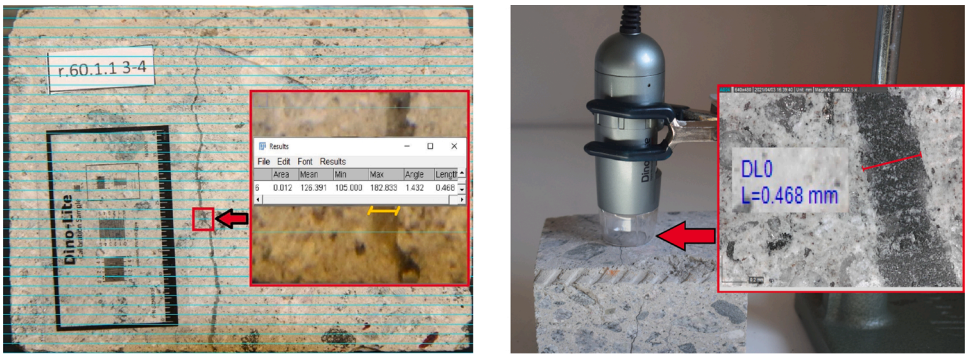

(a) (b)

Fig. 7. Measurement of crack widths using (a) DSLR camera photo with Fiji ImageJ program interface; (b) Direct observation with Dino-Lite digital microscope.

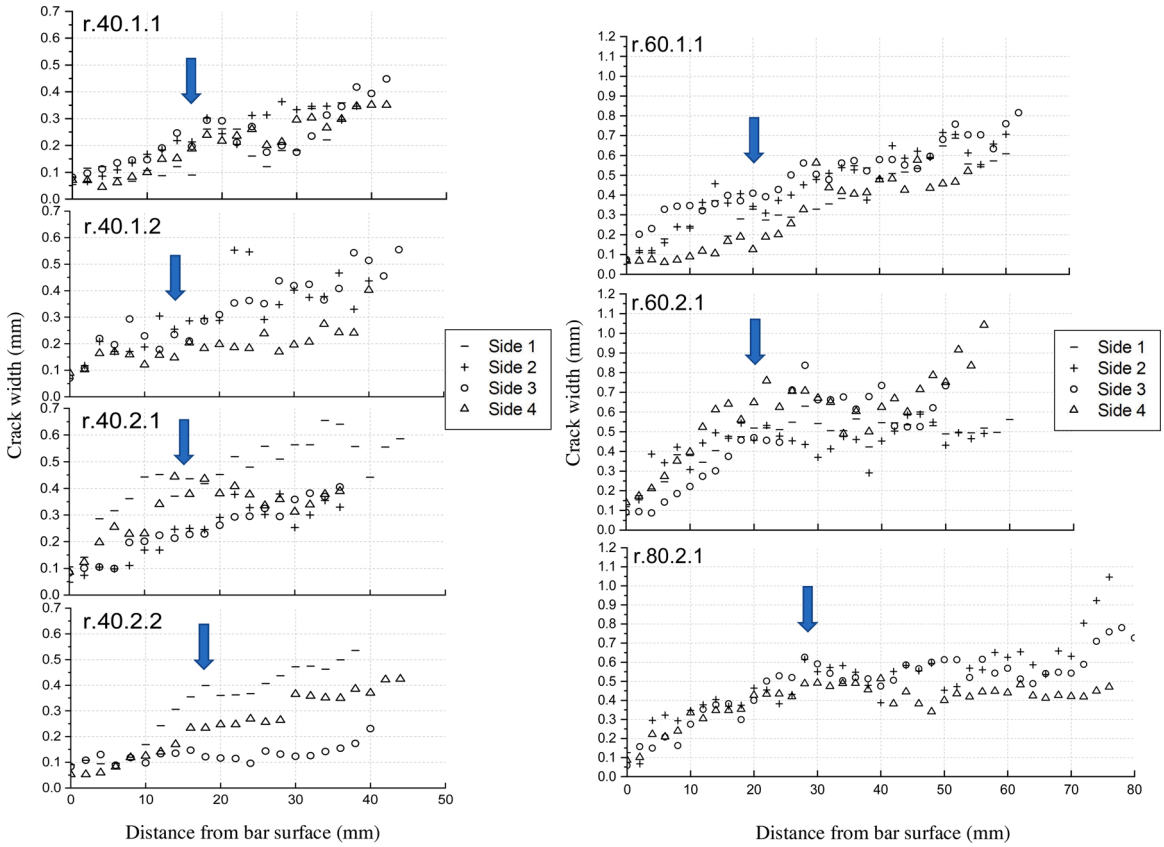

Fig. 8. Crack width variation along the concrete cover depth of the specimens with ribbed reinforcement.

cases, when more than one crack was generated in the tested specimen, two cracks were sealed. For example, in specimens r.40.1, r.40.2, s.20.1 and s.20.2, two cracks were sealed. Furthermore, specimen r.80.1 could not generate a crack, even when it was loaded up to the threshold value. Therefore, in the r.80.2 specimen, a 20-mm deep notch was made in side 1. Since the focus is to observe the crack width propagation along the concrete cover depth, crack width measurements were obtained from sides 2, 3 and 4. Further, in the specimens with smooth bars s.60.1 and s.60.2, no cracks could be obtained, as the specimens were not long enough. As can be observed in Figs. 8 and 9, it was not possible to obtain some measurements. In most of such cases, the specimen had been damaged while cutting. When the specimens are damaged, it is not possible to obtain a flat surface to measure the crack widths. This issue occurred more frequently in specimens with 20-mm cover depth. The measured crack width readings along the concrete cover depths are given in the Table A in attachment (Supplementary material).

4. Crack width variation along the concrete cover depth

Fig. 8 shows the crack width variation along the concrete cover depth of the SR. According to this figure, the crack width at the reinforcement is significantly smaller than the crack widths at the concrete surface. This observation is similar to the findings in the previously mentioned experiments reported in Tammo and Thelandersson [2,3], Yannopoulos [4], Husain and Ferguson [1], Beeby [5] and Borosnyoi and Snobli [6]. The crack width at the reinforcement is independent of the concrete cover depth, and, in all the cases, the crack width at the reinforcement showed a value below 0.1 mm. When considering the cases in Fig. 8, the rate of change in crack width, up to 10–30 mm from the reinforcement, is considerably higher than the rate of change in crack width beyond this limit. Borosnyoi and Snobli [6] and Caldentey et al. [10] have mentioned that this is due to the internal cracks (Goto cracks [11]), which are propagating up to this 10- to 30-mm limit. This limit of these internal cracks has been identified experimentally in Goto [11], and later considered in several studies like those of Debernardi et al. [12] and Debernardi and Taliano [13].

When primary cracks are developing, the tensile strain in reinforcement exceeds the ultimate tensile strain of the surrounding concrete [14]. This strain difference between the steel and concrete is referred to as ‘strain incompatibility’ in Beeby et al. [14]. Due to the good bond between the ribbed reinforcement and surrounding concrete, this strain incompatibility has been accumulated in the internal cracks. Further, it has been observed that this gradient changing point (arrow mark shown in Fig. 8) is moving slightly away from the reinforcement, with the increase in concrete cover depth. For specimens with 40-mm cover, this location lies within 10–18 mm; for specimens with 60-mm cover, this location lies around 20 mm; and, for specimens with 80-mm cover, this position lies around

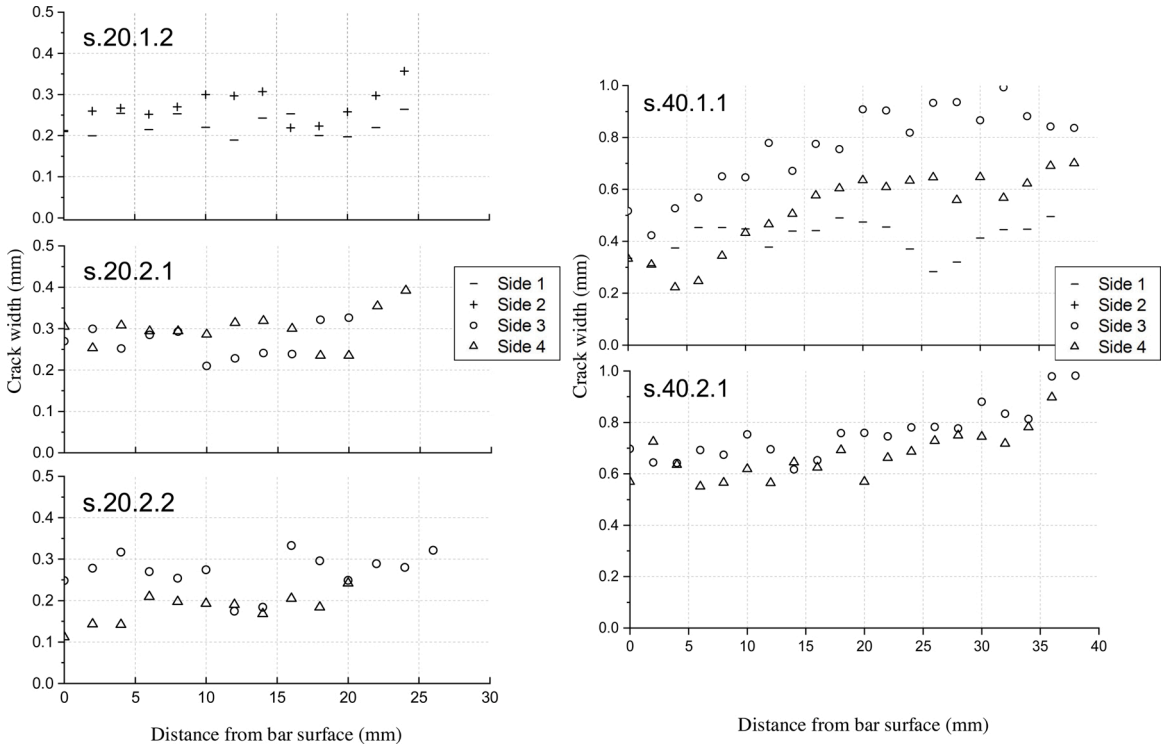

Fig. 9. Crack width variation along the concrete cover depth of specimens with smooth bars.

30 mm from the reinforcement. According to this discussion, which assumes that the internal cracks stop at the gradient changing point, the crack width at this gradient changing point can be considered to be due to the strain difference between reinforcement and concrete. When RC specimens are loaded from the reinforcement, the concrete within the cover depth (concrete between the bar and the concrete surface) is subjected to shear stress [20]. This shear stress would cause a shear deformation, which is referred to as 'shear lag'. According to Fig. 8, the crack widths are still increasing with a low gradient after the gradient changing point, and this can be considered to be due to this shear lag effect, as specified in several items of the literature [3,20,21].

The crack width variation of the SS differs considerably from that of the SR (Fig. 9). As shown in Fig. 9, crack width at the reinforcement is considerably larger than in the SR. The ratio between the surface crack widths and the crack width at the reinforcement of the SS varies from 1.2 to 2.2. On the other hand, unlike in the specimens with ribbed reinforcement, the rate of change in crack width at distance from the reinforcement is nearly the same throughout the concrete cover. Fig. 10 shows the actual view of crack width variation along the concrete cover depth of SR and SS of the specimens with 40-mm concrete cover depth. This implies that, as there are no ribs in the smooth bars, internal cracks are not dominant in these specimens (since the Goto cracks have initiated from the reinforcement ribs). Furthermore, as the crack width at the reinforcement is larger than in SR and the bond between smooth bars and surrounding concrete is comparatively low, it can be assumed that the strain incompatibility is accumulated by the occurrence of a slip [14].

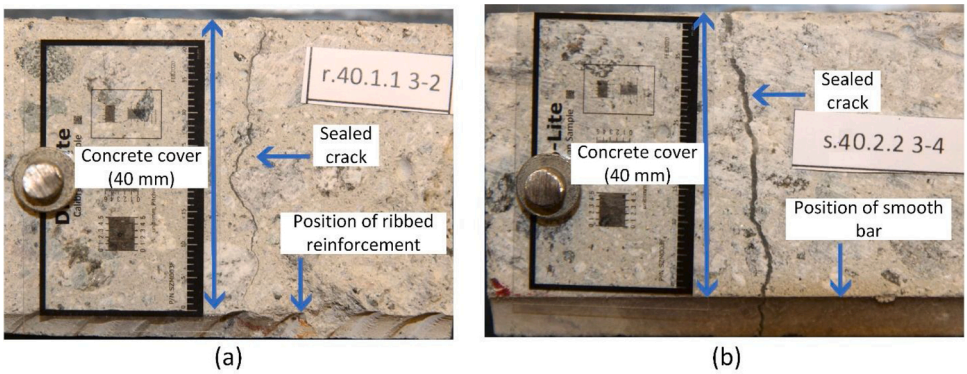

Fig. 10. Crack width variation along the concrete cover depth in specimens with 40-mm cover (a) with ribbed bars; (b) with smooth bars.

Crack width is considered to be the extension accumulated due to the strain difference between reinforcement and concrete within the crack spacing [7]. When considering the surface crack widths, the SS have larger surface crack widths than the SR (consider the specimens with 40-mm cover). This could be due to the SS consisting of larger crack spacings than the SR. Fig. 11 shows the crack position of each face of the tested RC specimens. It can be observed that the crack spacings of the specimens with smooth bars are larger than the crack spacings of the specimens with ribbed bars. This can be compared with the crack spacing results of the specimens with 40-mm cover depth. However, before comparing the crack spacing values in the SS and SR, it is important to mention that the loading conditions are not same in both type of specimens (Bar types are different and SS have loaded up to 80 kN and SR have loaded up to 100 kN). In the two specimens with ribbed bars, three cracks were obtained, while, in the two specimens with smooth bars, only a single crack was obtained. Similar behavior could be seen in the experiments reported in Randic and Markota [33]. Furthermore, many of the widely used crack width calculation models, like Eurocode 2 [8] and the JSCE model [34], predict that specimens with smooth bars

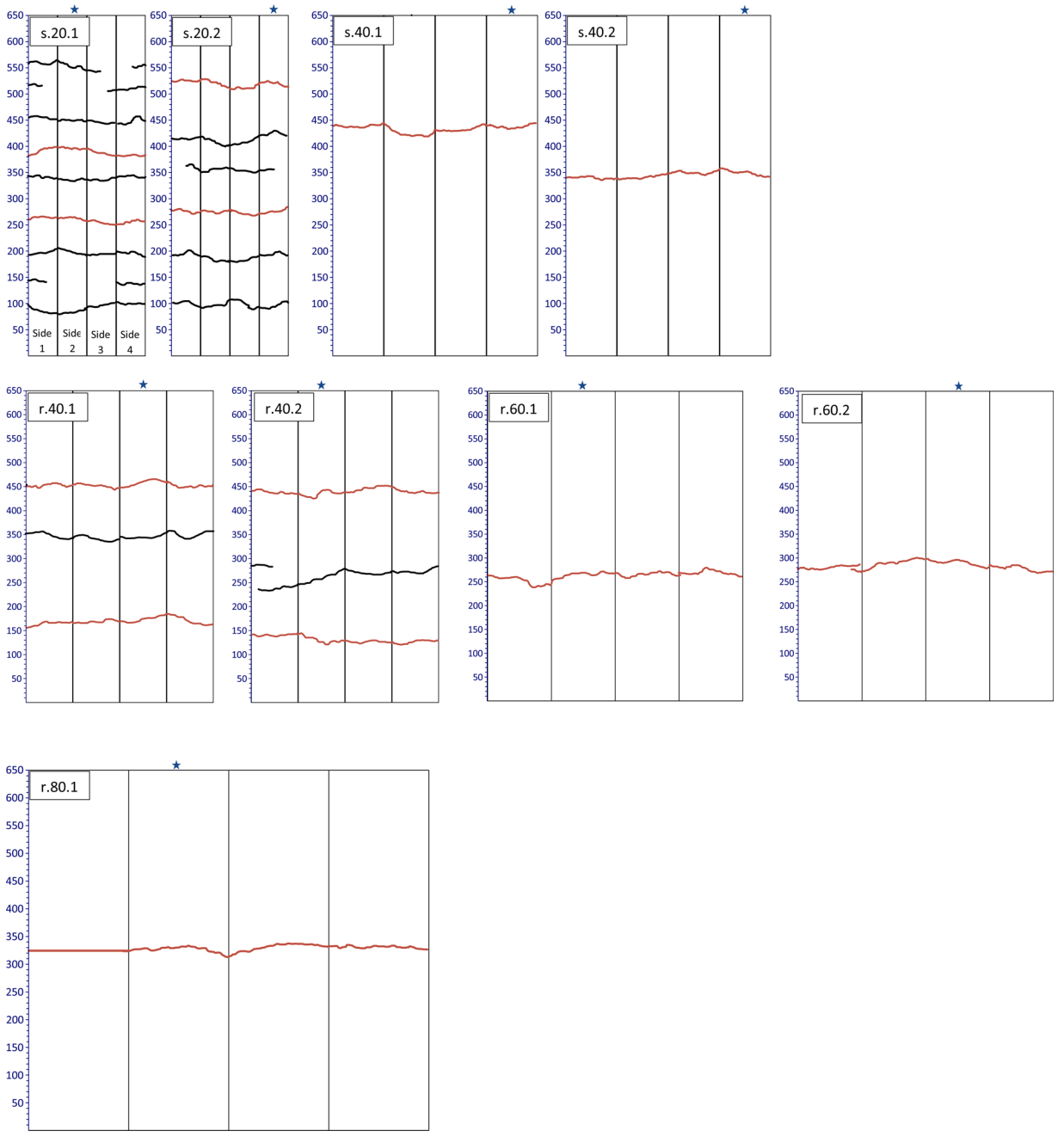

Fig. 11. Crack positions of the four sides of the tested RC specimens (sealed cracks are marked in red) and "star mark" shows the top surface during the concrete pouring.

have larger crack spacings than specimens with ribbed bars. Jakubovskis et al. [35] and Garcia et al. [36] studied the effect of concrete pouring directions on the cracking behavior. The top surface during the concrete pouring is marked with a * (star mark), in Fig. 11. Since it is not a primary objective of this study, the number of top surface during the concrete pouring differs in each specimen. When considering the results in Figs. 8, 9 and 11, no considerable influence could be observed on the crack widths and crack positions in the top surface during the concrete pouring of these tested specimens.

5. Applicability of bond-slip and no-slip theories for SR and SS

The no-slip theory assumes that the reinforcement and surrounding concrete are bonded perfectly [17]. Therefore, at the crack or at the ends of RC specimens, the stress is transferred to the surrounding concrete, according to St. Venant's principle [37]. According to St. Venant's principle, the next crack would occur after a certain distance (k × c distance; where 'k' is a constant and 'c' is concrete cover depth), when the stress in the concrete specimen is distributed uniformly along the cross section (Fig. 12(a)). The no-slip theory can explain the internal cracks, as they occur due to the strain incompatibility between reinforcement and concrete. When the surrounding concrete is strongly bonded with the reinforcement, and when applied tensile strain in the reinforcement exceeds the ultimate tensile strain of concrete, internal cracks can occur. On the other hand, if a slip occurs, internal cracks cannot be dominant.

According to Fig. 8, in almost all the SR, the crack widths at the reinforcement bar surface are less than 0.1 mm. This means that a negligible amount of slip has occurred between reinforcement and concrete. Therefore, in the SR, as a considerable amount of slip could not be observed, it can be assumed that the cracking behavior of the SR is more related to the no-slip theory. These negligible slip values in SR are evidently proved in the experimental studies focused on the bond-slip behaviors of axial tensile RC specimens, in Beconcini et al. [38], Doerr [39] and Bado et al. [40].

The bond-slip theory considers that a slip would occur between reinforcement and concrete. It is assumed that the slip is at its maximum at the crack and, after a certain distance, would become zero. Due to the slip, the concrete strain is not similar to the reinforcement strain. When the slip becomes zero, concrete strain is considered similar to the reinforcement strain [15] (Fig. 12(b)). When considering the force equilibrium for the concrete block between the crack and the zero slip section, the transfer length can be identified [12,16]. When considering the crack width variation of the SS, the crack width at the reinforcement bar surface is larger than that of the SR (Figs. 9 and 10(b)). The ratio of the average crack widths at the reinforcement bar surface of the SS to the SR is 3.8. Therefore, it can be assumed that a considerable amount of slip has occurred between reinforcement and concrete in the SS, comparatively to the SR. Further, unlike in the SR, during the experiment, a slip was clearly visible at the end of loaded specimens with smooth bars. Fig. 13 shows the reinforcement-concrete interface at the end of the SS, when it is loaded and unloaded. Therefore, the SS can be considered to behave more similarly to the bond-slip theory.

The importance of identifying the crack theory (no-slip or bond-slip theory) which is most related to the actual cracking behavior is that the crack spacing governing parameters are theoretically identified based on this theory. According to the no-slip theory, the governing crack spacing parameters can be considered to be concrete cover depth and the distance between tensile reinforcement (thickness of the surrounding concrete of the tensile reinforcement) [17,41]. For bond-slip theory, the governing crack spacing parameter can be considered to be bond parameter (ϕ/ρ; where 'ϕ' is the bar diameter and 'ρ' is the ratio between reinforcement area and concrete area) [12,16].

The conducted experimental program is focused on examining the crack widths. To study the crack spacings, relatively large specimen lengths are required, to avoid the end-effect encountered in short-length RC specimens [42]. However, Table 2 shows experimentally identified average crack spacings and the Eurocode 2 predictions. For this comparison, r.40, r.60, s.20 and s.40 specimens have been considered, since, in the r.80 specimens, the cracks have been induced. The experimental average crack spacing has been identified, by considering the specimen length and the number of cracks. The ratio of maximum crack spacing to average crack spacing considered in Eurocode 2 is 1.7 [43]. This ratio has been considered, to obtain the Eurocode 2 predicted average crack spicing values. For the SR and SS, the 'k_1' parameters in the Eurocode 2crack spacing model have been considered as 0.8 and 1.6, respectively. In the specimens used for this study, when the concrete cover depth increases, the value of the bond parameter (ϕ/ρ) also

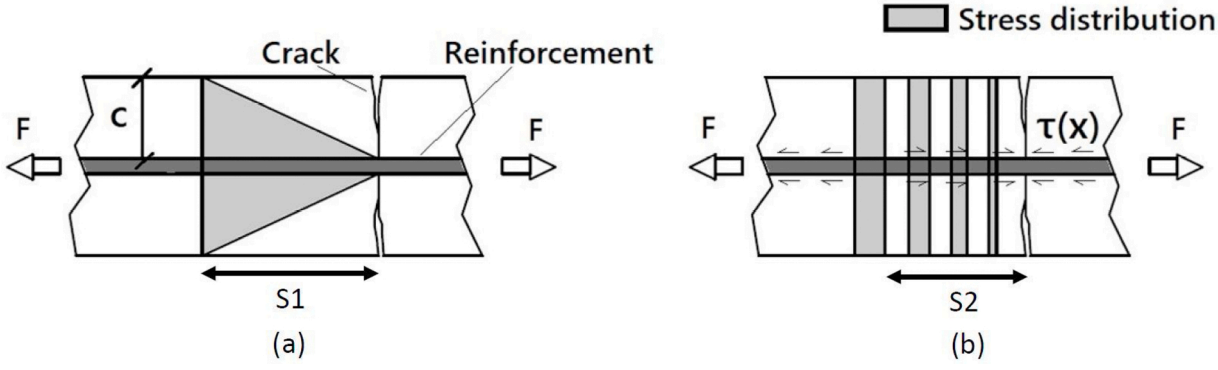

Fig. 12. Stress distribution in the concrete of a RC tie subjected to tension, according to (a) no-slip approach; (b) bond-slip approach.

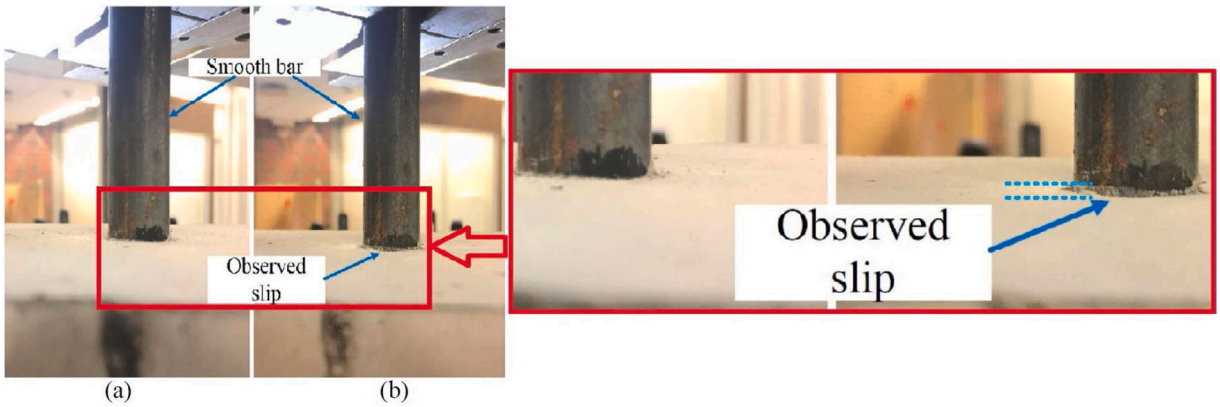

Fig. 13. Reinforcement-concrete interface at the end of the s.40.1 specimen (a) before; (b) after loading.

Table 2
Experimental and Eurocode 2 predicted average crack spacings.

Specimen	Cover (mm)	ϕ/ρ (mm)	Number of cracks	Average crack spacing (mm)	Eurocode 2 average crack spacing (mm)
r.40	40	733.8	3	163	227
r.60	60	1472.6	1	325	415
s.20	20	249.7	6	93	140
s.40	40	733.8	1	325	374

increases. As shown in Table 2, both experimental and Eurocode 2 predicted average crack spacings increased with the increase in concrete cover depth.

6. Derivation of the surface crack width calculation model for SR

Crack width calculation models, including Eurocode 2 and Model Code 2010, consider crack width as the extension accumulated due to the strain difference between reinforcement and concrete within the crack spacing [44]. Such models calculate the crack width by multiplying the crack spacing with the mean strain difference between reinforcement and concrete. These models assume a constant crack opening through the cover depth [6,9]. This implies that this method does not consider the effect of shear lag, which was discussed in Section 4. To identify whether the shear lag has an influence on surface crack width, the results of the conducted experimental program can be used. For this study, the crack spacing values can be directly obtained from the cracked specimens shown

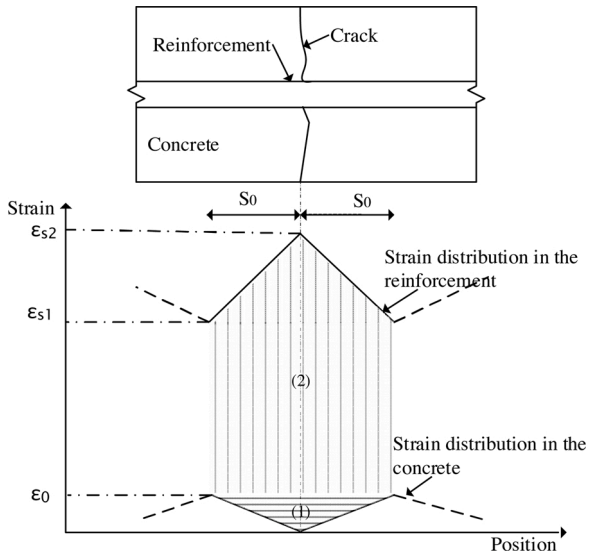

Fig. 14. Strain distribution of reinforcement and concrete at a crack in the stabilized cracking stage.

in Fig. 11. Strain difference between reinforcement and concrete can be calculated from Eurocode 2 or Model Code 2010 models. However, such models consist of several empirical coefficients. Therefore, for the purpose of this study, a crack width calculation model has been derived for the stabilized cracking stage, considering the results of previous experiments studying the strain in cracked RC specimens.

Beeby and Scott [14,45] have identified that the strain variation in steel on both sides of cracks is linear. In this series of experiments mentioned in Beeby and Scott [14,45], the steel strains were measured in 10-mm gaps. Since a linear strain distribution has been observed in every tested specimen, this behavior is considered in the development of the crack width calculation model. Similar observations (linear strain distribution in reinforcement on both sides of the crack) could be observed in the experiments in Kankam [46] and Imai et al. [47]. Since the reinforcement strain is linear, by considering the force equilibrium, it has been assumed that the concrete strain is also linear on both sides of cracks [14]. Fig. 14 shows the strain distribution of reinforcement and concrete in both sides of a crack at the stabilized cracking stage, based on the results of the aforementioned literature.

Crack width can be considered the summation of the contraction of concrete and the extension of the reinforcement in the region of the crack [14]. For the purpose of calculation, it is assumed that the region of the crack is the region within S_o distance from both sides of the crack (Fig. 14).

Extension of the reinforcement within the region of the crack, due to the increment of reinforcement stress (Area (2) in Fig. 14):

$$\Delta_s = \frac{1}{2}\left[(\varepsilon_{s1} - \varepsilon_0) + (\varepsilon_{s2} - \varepsilon_0)\right] S_0 \,.\, 2 \tag{1}$$

where ε_{s1} is the steel strain at the end of the transfer length in the stabilized cracking stage, ε_{s2} is the steel strain at the crack in the stabilized cracking stage, ε_0 is the concrete strain at the end of the transfer length, and S_0 is the transfer length.

Theoretically, ε_{s1} can be written as '$\varepsilon_{s2} - \alpha_e\varepsilon_0$' [48]. Therefore, Eq. (1) can be rearranged as:

$$\Delta_s = [2.\varepsilon_{s2} - \varepsilon_0(2 + \alpha_e)]\ S_0 \tag{2}$$

where α_e is the modular ratio.

Contraction of the concrete (Δ_c) within the region of the crack due to the reduction of concrete stress in the crack (Area (1) in Fig. 14):

$$\Delta_c = S_0\ \varepsilon_0 \tag{3}$$

Crack width (w) is the summation of the contraction of concrete (Δ_c) and the extension of the reinforcement (Δ_s) in the region of the crack. Therefore, crack width at the stabilized cracking stage can be obtained from:

$$w = \Delta_c + \Delta_s \tag{4}$$

$$w = 2\ S_0\left[\varepsilon_{s2} - \frac{\varepsilon_0(1 + \alpha_e)}{2}\right] \tag{5}$$

where '2 S_0' can be considered the crack spacing and α_e is the modular ratio.

$$\varepsilon_{s2} = \sigma_s/E_s \tag{5-a}$$

where σ_s is the steel stress, and E_s is the Young's modulus of steel.

$$\varepsilon_0 = \frac{N_{cr}}{E_c A_{c,eff}(1 + \alpha_e\rho)} \tag{5-b}$$

where N_{cr} is the cracking force, E_c is the Young's modulus of concrete, $A_{c,\,eff}$ is the effective concrete area, α_e is the modular ratio, and ρ is the ratio of reinforcement area to effective concrete area.

$$N_{cr} = \sigma_{sr}\ A_s \tag{5-c}$$

where σ_{sr} is the maximum steel stress at cracking force, and A_s is the reinforcement area.

When the cracked section is considered, concrete cannot resist tensile stresses at the crack (neglecting the cracked concrete softening effect). Therefore, the maximum steel stress at the cracking force can be obtained from the following equation:

$$\sigma_{sr} = f_{ctm}\left(A_{c.eff}/A_s\right) + f_{ctm}\left(E_s/E_c\right) \tag{5-d}$$

where f_{ctm} is the mean tensile strength of concrete.

Eq. (5-d) can be rearranged according to Eq. (5-e), with familiar notations as represented in Model code 2010.

$$\sigma_{sr} = \frac{f_{ctm}}{\rho_{p,eff}}\ (1 + \alpha_e\rho_{p,eff}) \tag{5-e}$$

where $\rho_{p,eff}$ is the effective reinforcement ratio ($\rho_{p,eff} = A_s/A_{c,\,eff}$)

Eq. (5) is developed assuming the concrete strain is distributed uniformly along the concrete cover depth. However, in order to obtain the surface crack widths, the effect of shear-lag can be considered [3,14,21]. Therefore, in order to quantify this effect, the calculation model given in the 'fib Model Code first complete draft' [21] has been considered, following a modification, as shown in Eq. (6).

$$w = \left[S + 1.7\,(c-a)\right]\left[\varepsilon_{s2} - \frac{\varepsilon_0(1+\alpha_e)}{2}\right] \tag{6}$$

where 'S' is the crack spacing value, 'c' is the concrete cover depth and 'a' is the distance to the gradient changing point from the reinforcement surface (15, 20 and 30 mm for cover depths of 40, 60 and 80 mm, respectively).

It has introduced a parameter, 'a', which is the distance to the gradient changing point from the reinforcement surface, instead of the 25-mm value which was originally in the model. According to this study, the distance, 'a', depends on the concrete cover depth (the arrow marked in Fig. 8). For calculation purposes, in specimens with cover depths of 40, 60 and 80 mm, the 'a' value can be considered as 15, 20 and 30 mm, respectively. For those cases where the concrete cover depth is other than the mentioned values, the 'a' distance can be considered by interpolation.

7. Comparison of surface crack widths with the calculated crack widths of the SR

The surface crack width is considered the crack width at the concrete surface over the axis of the reinforcement [9]. As shown in Fig. 5, the crack width variation along the concrete cover depth is also considered along the reinforcement axis. Therefore, the measured surface crack width can be obtained as the concrete surface readings from Fig. 8. For better comparison, the crack width predictions of both Eurocode 2 and Model Code 2010 have been considered. Crack width calculation models in these two codes calculate the crack width by multiplying the crack spacing with the mean strain difference. At the stabilized cracking stage, both standards calculate the mean strain difference according to Eq. (7) (without considering the shrinkage strain term mentioned in Model Code 2010). Both the mean strain difference in Eq. (7) and the strain term in Eqs. (5) and (6) can be calculated with the data from the experiment. For the calculated crack widths from Eq. (8), the parameter k_t, which is used for the duration of load, is considered as 0.4, as suggested by both codes for short-term loadings.

$$\varepsilon_{sm} - \varepsilon_{cm} = \frac{\sigma_s - k_t\left(f_{ct,eff}/\rho_{p,eff}\right)(1+\alpha_e\rho_{p,eff})}{E_s} \tag{7}$$

$$w = S\,.\,(\varepsilon_{sm} - \varepsilon_{cm}) \tag{8}$$

where '$\varepsilon_{sm} - \varepsilon_{cm}$' is the mean strain difference between reinforcement and concrete; '$f_{ct,\,eff}$' is the mean tensile strength of concrete, effective at the time when the test is performed; '$\rho_{p,eff}$' is the effective reinforcement ratio; 'w' is the crack width; and 's' is the crack spacing value.

The experimental surface crack widths have been compared with the predictions of Eqs. (5), (6) and (8). Eqs. (5) and (8) are developed without considering the effect of shear lag, while Eq. (6) considers the effect of shear lag. For this study, the necessary crack spacing values required for the crack width prediction equations were directly obtained by measuring from the cracked specimens (refer to Fig. 9). The crack spacing value corresponding to a specific crack can be considered as the summation of halves of crack distances to both sides of the cracks (refer to Fig. 14) [44]. It is important to mention that this method of measuring crack spacing is considered only for this study, where the focus is on the width of a specific crack. On the other hand, when developing the basic crack width calculation models in Eurocode 2 and Model Code 2010, the cracking region of a specific crack was identified, based on this method [44]. In the SR, a total number of seven cracks were sealed. For each crack, the surface crack widths and crack positions corresponding to the four surfaces are different from each other (refer to Figs. 8 and 9). Therefore, altogether there is data on 28 (7×4) surface crack widths. However, as some specimens were damaged while cutting the specimens, 26 surface crack widths were considered for this comparison.

The graph of the measured surface crack width versus calculated crack width, using Eqs. (5) and (8), is shown in Fig. 15. The code models are used to verify whether the values of the theoretical crack widths are safe or not, and their purpose is to not to predict exact crack widths. The predictions of Eq. (8) have been considered for this study only as a reference to the predictions of Eq. (5). The mean absolute error (the average of the absolute difference between the measured value and the predicted value) of the predictions from Eqs. (5) and (8) is 0.12 and 0.11, respectively. Fig. 15 shows that there are several calculated crack widths consistent with a constant value. This is because, according to the aforementioned crack spacing measuring method, the crack spacing values of the specimens with a single crack will be 325 mm for every case (half of the specimen size). This figure shows that, for the majority of cases, the predictions of Eqs. (5) and (8) are underestimating the experimental surface crack width. From a total of 26 cases, 16 cases from both Eqs. (5) and (8) predict underestimated crack width values, compared to the experimental observations. Eq. (8) is the crack width prediction model in Eurocode 2. Therefore, in order to predict conservative crack width values, this can be the reason that the Eurocode 2 crack spacing model predicts significantly overestimated crack spacing values to calculate the crack widths [19,48,49]. Fig. 16 shows the comparison of the measured surface crack widths with the predictions from Eq. (6), which have considered the effect of shear lag. The mean absolute error of the predictions from Eq. (6) is 0.15. According to these Eq. (6) predictions, only 8 out of 26 cases underestimate the

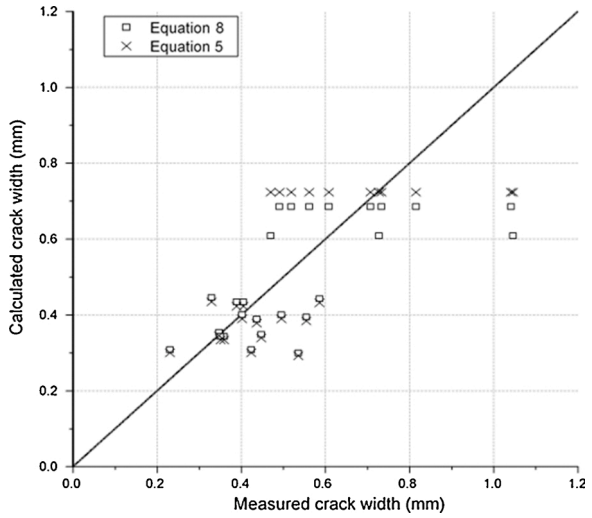

Fig. 15. Comparison of the measured surface crack widths of SR with Eqs. (5) and (8) (models do not consider the shear lag effect).

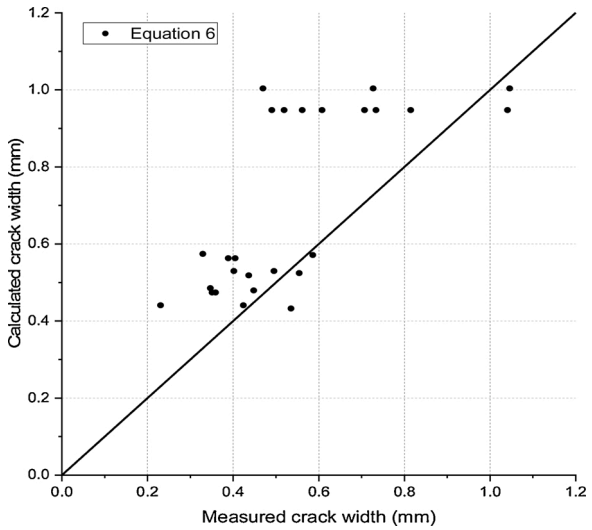

Fig. 16. Comparison of the measured surface crack widths of SR with Eq. (6) (equation with the shear lag effect).

experimental crack widths.

This comparison shows the importance of the effect of shear lag on the surface crack widths. However, this study has been conducted for a limited number of results. Therefore, this must be further verified with RC specimens with different types of concrete, sizes of bar diameters and cover depths. For that, exact crack widths (not average values), and the exact crack spacing values correspond to each crack, are required. Therefore, despite the large body of literature available on crack width studies, the experimental program mentioned in Gribniak et al. [50], which includes the aforementioned data, was selected. Further, it is important to mention that this 'a' value is obtained only for short-length concrete prisms reinforced with a central bar (the conducted experimental program). However, these values must be further verified with the practical size members, due to the identified end-effect encountered in short-length RC specimens [42]. To verify the proposed equations, the results in Gribniak et al. [50] were compared with the predictions of the proposed models (Eqs. (5) and (6)). For this comparison, the results of 1210-mm-long RC specimens with identical 150 × 150-mm cross sections were considered. The cover depths of the selected RC specimens were 30 mm, 40 mm and 50 mm, and they were reinforced with four 10-mm bars. Depending on the availability of data, the results of 3, 2 and 2 specimens, with concrete cover depths of 50 mm, 40 mm and 30 mm, respectively, were selected. In this experiment, the crack widths were measured at the concrete surface above the positions of the reinforcement bars. For this study, the crack widths when the applied load is 100.4 K N were considered. These crack widths were measured using the DIC (Digital Image Correlation) system. As specified in Section 6, the 'a' values have considered to be 17.5 mm, 15 mm and 12.5 mm for specimens with 50 mm, 40 mm and 30 mm covers, respectively. Fig. 17 shows the graph of the measured surface crack width versus calculated crack width, using Eqs. (5) and (6), and the Table B in

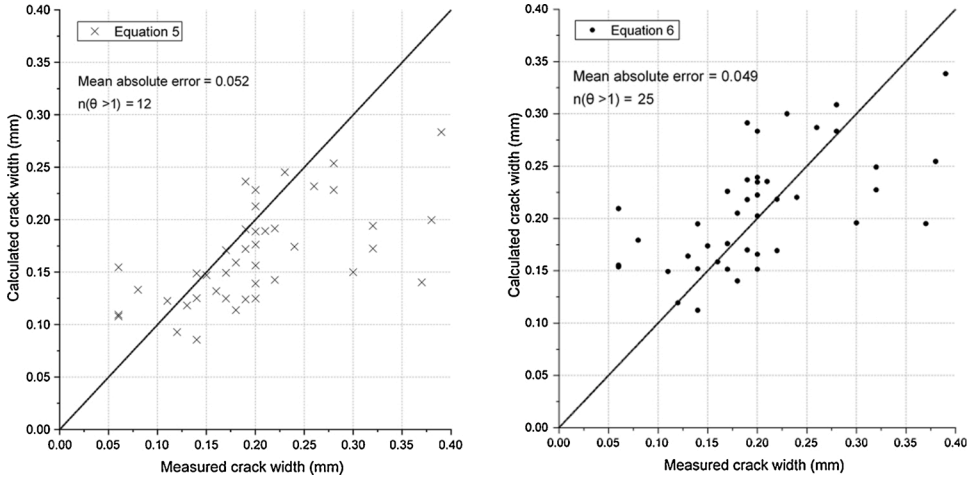

Fig. 17. Comparison of the measured surface crack widths in Gribniak et al [50] with the predictions from (a) Eq. (5), and (b) Eq. (6). 'n($\theta > 1$)' notation represent the number of conservative predictions out of 42 cases, where calculated crack width is greater than the measured crack width.

Attachment (Supplementary material) shows the calculated and measured crack width values. The mean absolute error values for the predictions of Eqs. (5) and (6) are 0.052 and 0.049, respectively. When considering the 42 cases mentioned in Fig. 17, according to the Eq. (5), only 12 cases and according to the Eq. (6), 25 cases give conservative predictions (calculated crack width is greater than the measured crack width). Therefore, the proposed Eq. (6), which includes the shear-lag effect, gives better agreement with the experimental results than Eq. (5) does.

8. Conclusions

To understand the cracking behavior of RC specimens, crack width variation along the concrete cover depth was studied. An experimental program was conducted, using concrete prisms reinforced with a central bar. RC specimens were cast with both ribbed bars and smooth bars and with different concrete cover depths. These specimens were tested by applying an axial tensile load, and the generated cracks were sealed by using a high-strength and low viscosity epoxy. After the epoxy had hardened, the cracked specimens were cut and the crack width propagation along the concrete cover depth observed. The following observations and understandings can be obtained from this study.

- When considering the specimens with ribbed bars (SR), the ratios of average surface crack width to average crack width, at the reinforcement surface in each crack, vary from five to ten. The crack width difference between reinforcement bar surface and concrete surface can be identified as being due to the internal cracks which occur at the vicinity of the primary crack. In SR, the strain incompatibility that occurs between reinforcement and concrete accumulates in the internal cracks. On the other hand, a negligible amount of slip could be observed between these ribbed bars and the surrounding concrete. This can be considered to be due to the good bond between the ribbed reinforcement and the concrete.
- In the specimens with smooth bars (SS), the average crack width at the reinforcement bar surface is almost four times larger than that of the specimens with ribbed bars. Since the crack width varies linearly along the cover depth, it is assumed that there is no significant effect from the internal cracks. Therefore, in the SS, it can be assumed that the strain incompatibility between reinforcement and concrete has been accommodated by a slip.
- It is important to identify the crack theory (bond-slip theory or no-slip theory) which is more relevant to the actual cracking behavior of the RC specimens, because the crack spacing governing parameters are mainly identified based on these theories. Therefore, according to the experimental results, it can be stated that specimens with ribbed bars behave in a way more related to the no-slip theory, while specimens with smooth bars behave in a manner more related to the bond-slip theory.
- A surface crack width prediction model has been developed by considering the effect of shear lag. A simple study has been conducted, to compare the experimental surface crack widths with the predictions from models which do consider and do not consider the shear-lag effect. The end results have shown that the shear-lag effect has an influence on surface crack widths. However, this study must be further verified for RC specimens with different concrete properties, bar diameters and concrete covers.

Declaration of Competing Interest

The authors report no declarations of interest.

Acknowledgements

The authors would like to thank the University of Stavanger laboratory manager, John C. Grønli, laboratory engineers, Jarle Berge and Samdar Kakay, as well as Johannes Jensen, for the variety of support given during the experiments. Further, the authors would like to thank Mikko Mathias, Espen Sorensen and William Bui for the variety of support given regarding specimen preparations.

Appendix A. Supplementary data

Supplementary material related to this article can be found, in the online version, at doi:https://doi.org/10.1016/j.cscm.2021.e00593.

References

[1] S.I. Husain, P.M. Ferguson, Flexural Crack Width at the Bars in Reinforced Concrete Beams, The University of Texas at Austin, Center for Highway research, 1968.
[2] K. Tammo, S. Thelandersson, Crack opening near reinforcement bars in concrete structures, Struct. Concr. 7 (4) (2006) 137–143.
[3] K. Tammo, S. Thelandersson, Crack behavior near reinforcing bars in concrete structures, ACI Struct. J. 106 (3) (2009) 259.
[4] P. Yannopoulos, Variation of concrete crack widths through the concrete cover to reinforcement, Mag. Concr. Res. 41 (147) (1989) 63–68.
[5] A. Beeby, Corrosion of reinforcing steel in concrete and its relation to cracking, Struct. Eng. 56 (3) (1978).
[6] A. Borosnyói, I. Snóbli, Crack width variation within the concrete cover of reinforced concrete members, Építõanyag 62 (3) (2010) 70–74.
[7] G.L. Balazs, Cracking analysis based on slip and bond stresses, Mater. J. 90 (4) (1993) 340–348.
[8] E.C.f. Standardization, Eurocode 2: Design of Concrete Structures - Part 1–1: General Rules and Rules for Buildings, 2004.
[9] I.F.f.S.C. (fib), fib Model Code for concrete structures. Structural Concrete, 2010.
[10] A. Pérez Caldentey, H. Corres Peiretti, J. Peset Iribarren, A. Giraldo Soto, Cracking of RC members revisited: influence of cover, ϕ/ρs, ef and stirrup spacing–an experimental and theoretical study, Struct. Concr. 14 (1) (2013) 69–78.
[11] Y. Goto, Cracks formed in concrete around deformed tension bars, ACI J. Proc. (1971) 244–251.
[12] P.G. Debernardi, M. Guiglia, M. Taliano, Effect of secondary cracks for cracking analysis of reinforced concrete tie, ACI Mater. J. 110 (2) (2013) 207.
[13] P.G. Debernardi, M. Taliano, An improvement to Eurocode 2 and fib Model Code 2010 methods for calculating crack width in RC structures, Struct. Concr. 17 (3) (2016) 365–376.
[14] A. Beeby, R. Scott, Cracking and deformation of axially reinforced members subjected to pure tension, Mag. Concr. Res. 57 (10) (2005) 611–621.
[15] R. Saliger, High grade steel in reinforced concrete, Second Congress of IABSE (1936). IABSE Publications, Berlin-Munich.
[16] M. Taliano, Cracking analysis of concrete tie reinforced with two diameter bars accounting for the effect of secondary cracks, Eng. Struct. 144 (2017) 107–119.
[17] B.B. Broms, Crack width and crack spacing in reinforced concrete members, ACI J. Proc. 62 (10) (1965) 1237–1256.
[18] J.F. Borges, Cracking and Deformability of Reinforced Concrete Beams, Laboratório Nacional de Engenharia Civil, 1965.
[19] C.N. Naotunna, M.K.S.S.M. Samindi, K.T. Fosså, Experimental and theoretical behavior of crack spacing of specimens subjected to axial tension and bending, Struct. Concr. 1 (18) (2020).
[20] A. Beeby, C. Alander, E. Giuriani, G. Plizzari, S. Pantazopoulou, The influence of the parameter ϕ/ρeff on crack widths. Author's reply and discussion, Struct. Concr. (Lond. 1999) 6 (4) (2005) 155–165.
[21] J. Walraven, Model Code 2010-First Complete Draft-Volume 2: Model Code, fib Fédération Internationale du Béton, 2010.
[22] G. Markeset, M. Kioumarsi, Need for further development in service life modelling of concrete structures in chloride environment, Procedia Eng. 171 (2017) 549–556.
[23] J. Connal, M. Berndt, Sustainable bridges: 300 year design life for Second Gateway Bridge, in: 7th Austroads Bridge Conference, Auckland, New Zealand, 2009.
[24] NPRA, Statens Vegvesen. Håndbok N400 Bruprosjektering, Vegdirektoratet, Oslo, 2009.
[25] M. Basteskår, M. Engen, T. Kanstad, K.T. Fosså, A review of literature and code requirements for the crack width limitations for design of concrete structures in serviceability limit states, Structural Concrete 20 (2) (2019) 678–688.
[26] NS, EN 3576-3, Steel for the Reinforcement of Concrete - Dimensions and Properties - Part 3: Ribbed Steel B500NC, 2012.
[27] NS, EN 10219, Cold Formed Welded Structural Hollow Sections of Non-Alloy and Fine Grain Steels, Part 1: Technical Delivery Conditions, 2006.
[28] E. Cadoni, D. Forni, R. Gieleta, L. Kruszka, Tensile and compressive behaviour of S355 mild steel in a wide range of strain rates, Eur. Phys. J. Spec. Top. 227 (1) (2018) 29–43.
[29] A. Duarte, B. Silva, N. Silvestre, J. De Brito, E. Júlio, J. Castro, Tests and design of short steel tubes filled with rubberised concrete, Eng. Struct. 112 (2016) 274–286.
[30] EN, 1504-5: 2004, Products and Systems for the Protection and Repair of Concrete Structures, Definitions, Requirements, Quality Control and Evaluation of Conformity. Concrete Injection, 2004.
[31] C.A. Schneider, W.S. Rasband, K.W. Eliceiri, NIH Image to ImageJ: 25 years of Image analysis, Nat. Methods 9 (7) (2012) 671–675.
[32] M. Amato, F. Lupo, G. Bitella, R. Bochicchio, M.A. Aziz, G. Celano, A high quality low-cost digital microscope minirhizotron system, Comput. Electron. Agric. 80 (2012) 50–53.
[33] J. Radnić, L. Markota, Experimental verification of engineering procedures for calculation of crack width in concrete elements, Int. J. Eng. Model. 16 (2003) 63–69.
[34] JSCE, Standard Specifications for Concrete Structures-2007, Design, Japanese Society of Civil Engineers Guidelines for Concrete, 2007.
[35] R. Jakubovskis, R. Kupliauskas, A. Rimkus, V. Gribniak, Application of FE approach to deformation analysis of RC elements under direct tension, Struct. Eng. Mech. 68 (3) (2018) 345–358.
[36] R. García, A.P. Caldentey, Influence of type of loading (tension or bending) on cracking behaviour of reinforced concrete elements. Experimental study, Eng. Struct. 222 (2020), 111134.
[37] M. de Saint-Venant, Mémoire sur la torsion des prismes: avec des considérations sur leur flexion ainsi que sur l'équilibre intérieur des solides élastiques en général: et des formules pratiques pour le calcul de leur résistance à divers efforts s' exerçant simultanément, Imprimerie National, 1856.
[38] M.L. Beconcini, P. Croce, P. Formichi, Influence of bond-slip on the behaviour of reinforced concrete beam to column joints, Proceedings of International fib Symposium (2008) 19–21. Taylor Made Concrete Structures: New Solutions for our Society, Amsterdam.
[39] K. Doerr, Bond behavior of ribbed reinforcement under transversal pressure, Nonlinear Behavior of Reinforced Concrete Structures; Contributions to IASS Symposium (1978) 3–7.
[40] M.F. Bado, J.R. Casas, G. Kaklauskas, Distributed Sensing (DOFS) in reinforced concrete members for reinforcement strain monitoring, crack detection and bond-slip calculation, Eng. Struct. 226 (2020), 111385.
[41] B.B. Broms, L.A. Lutz, Effects of arrangement of reinforcement on crack width and spacing of reinforced concrete members, ACI J. Proc. (1965) 1395–1410.
[42] V. Gribniak, A. Rimkus, L. Torres, R. Jakstaite, Deformation analysis of reinforced concrete ties: representative geometry, Struct. Concr. 18 (4) (2017) 634–647.

[43] C. Braam, Control of Crack Width in Deep Reinforced Concrete Beams [Dissertation], Delft University of Technology, Netherlands, 1990.
[44] A. Beeby, Crack control provisions in the new eurocode for the design of concrete structures, ACI Spec. Publ. 204 (2001) 57–84.
[45] A.W. Beeby, R.H. Scott, Influence of Tension Stiffening on Deflection of Reinforced Concrete Structures: Report of a Concrete Society Concrete Society Technical Report, Camberley, 2003.
[46] C.K. Kankam, Relationship of bond stress, steel stress, and slip in reinforced concrete, J. Struct. Eng. 123 (1) (1997) 79–85.
[47] M. Imai, R. Nakano, T. Kono, T. Ichinomiya, S. Miura, M. Mure, Crack detection application for fiber reinforced concrete using BOCDA-based optical fiber strain sensor, J. Struct. Eng. 136 (8) (2010) 1001–1008.
[48] R. Tan, K. Eileraas, O. Opkvitne, G. Žirgulis, M.A. Hendriks, M. Geiker, D.E. Brekke, T. Kanstad, Experimental and theoretical investigation of crack width calculation methods for RC ties, Struct. Concr. (2018) 1436–1447.
[49] R. Tan, Consistent Crack Width Calculation Methods for Reinforced Concrete Elements Subjected to 1D and 2D Stress States A Mixed Experimental, Numerical and Analytical Approach, Norwegian University of Science and Technology, Trondheim, Norway, 2019.
[50] V. Gribniak, A. Rimkus, A.P. Caldentey, A. Sokolov, Cracking of concrete prisms reinforced with multiple bars in tension–the cover effect, Eng. Struct. 220 (2020), 110979.